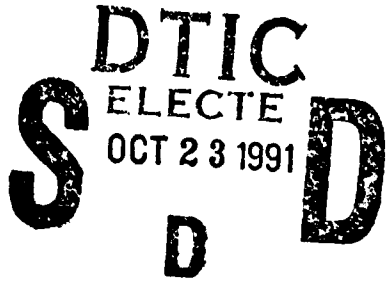


Office of the Chief of Naval Research
Contract N00014-87-K-0326
Technical Report No. UWA/DME/TR-91/7

# Dynamic Fracture Characterization of $Al_2O_3$ and $SiC_w/Al_2O_3$

**L.R. Deobald and A.S. Kobayashi**



September 1991

The research reported in this technical report was made possible through support extended to the Department of Mechanical Engineering, University of Washington, by the Office of Naval Research under Contract N00014-87-K-0326. Reproduction in whole or in part is permitted for any purpose of the United States Government.

# Dynamic Fracture Characterization of $Al_2O_3$ and $SiC_w/Al_2O_3$

L.R. Deobald and A.S. Kobayashi

**Abstract:**

Rectangular bars of $Al_2O_3$ and 29% volume fraction SiC whisker/$Al_2O_3$ composite with sharp precracks were tested with newly developed bar impact facilities and a new data reduction procedure. The fracture surface morphology was studied with a scanning electron microscope (SEM) and compared with the impact velocity and the dynamic stress intensity factor ,$K_I^{dyn}$, history.

The crack propagation history and $K_I^{dyn}$ curves for the $Al_2O_3$ and 29% v. $SiC_w/Al_2O_3$ composite were virtually the same indicating that the short SiC whiskers were ineffective under dynamic fracture. SEM study revealed five distinct fracture morphology regions with increased percentage area of transgranular fracture in the ceramic matrix of both the $Al_2O_3$ and the $SiC_w/Al_2O_3$ with rapid crack propagation. Also the high dynamic stress intensity factor caused multiple microscopic crack planes to form and then join as the crack advanced.

## 1. Introduction

In spite it's many favorable properties, ceramics has severe disadvantages of brittleness and poor impact resistance due to it's inherently low fracture toughness. An obvious method to improve the toughness of ceramic materials is through the use of composite techniques. The possible improved toughness due to the added ceramic whisker/fibers should allow a "graceful" failure rather than the catastrophic failure of a ceramic component. Several mechanisms exist by which a ceramic matrix composite can exhibit superior toughness over the toughness of the matrix material. These mechanisms include crack bridging, fiber pullout, crack deflection mechanisms, microcrack shielding, and phase transformation[1]. In crack bridging, intact whisker fibers bridge the space between the two crack faces of the matrix. Since the fibers apply a crack closure force behind the crack tip, addition energy is required to overcome this force and propagate the crack. The fiber pullout mechanism absorbs additional fracture energy by dissipating energy through friction as a broken fiber is pulled from the matrix. A crack will deflect around a whisker due to an altered stress field which may either be caused by a difference in the coefficient of thermal expansion between the two phases or by a difference in the elastic moduli. In the following, experimental studies on the stress intensity factor for the onset of rapid crack propagation, $K_{Id}$, and the propagating stress intensity factor, $K_I^{dyn}$, under dynamic loading for a ceramic composite and its matrix material are presented and possible micromechanic causes for the observed dynamic responses are discussed.

## 2. Experimental Procedure

The two quantities measured were the COD history and the stress history. The stress history was measured using a strain gage located at the middle of the ceramic bar. The COD history was measured with the laser interferometric displacement gage (LIDG) technique[2,3].

A schematics of the LIDG used for this particular experiment is shown in Figure 1. The change in the crack opening displacement (COD) is registered as fringe motion at the two photomultiplier tubes (PMT) which were positioned at an angle of $\Theta$ on either side of the indentation pair. The change in displacement is then predicted by Equation (1), where $\delta m_1$ and $\delta m_2$ represent changes in fringe orders.

$$\Delta d = \frac{(\delta m_1 + \delta m_2)\lambda}{2 \sin \Theta} \qquad (1)$$

The Vickers indentation produced a reflection at $\Theta$=44° and the 10 mW helium-neon laser has a wave length $\lambda$ of 632.8 nm. The sensitivity of this particular technique is 0.911 mm per fringe. The fringe motion measurement was required on either side of the indentation pair in order to subtract out rigid body motions.

The specimen geometry is shown in Figure 1. A sharp precrack with an approximate initial length of 3 mm was introduced at the midplane of the bar using the single-edge-precracked-beam (SEPB)[4,5] method. A strain gage with short 1.6 mm gage length was mounted in front of the precrack, also at the bar's midplane. A metal foil for the LIDG method was mounted on the adjacent surfaces such that a cut in the center of the foil was aligned with the precrack. The foil was then polished and indented with the Vickers microhardness indentor which produced targets for the LIDG technique spaced 0.4 mm apart.

The two materials listed in Table 1, i.e. $Al_2O_3$ and 29% vol. $SiC_w/Al_2O_3$, were studied. The monolithic $Al_2O_3$ is the matrix material for the CMC.

Table 1, Mechanical properties of $Al_2O_3$ and 29% vol. $SiC_w/Al_2O_3$.

| Material | E (GPa) | $\nu$ | $\rho$ (g/cc) | $K_{IC}$ (MPa$\sqrt{m}$)* |
|---|---|---|---|---|
| $Al_2O_3$ 99.9% | 387 | .22 | 3.97 | 4 |
| 29% v $SiC_w/Al_2O_3$ | 408 | .23 | 3.73 | 7 |

*From static fracture toughness measurements.

Schematics of the impact apparatus and the air gun are shown in Figure 2. The specimen and impactor are held by molded urethane holders which are mounted in carriages. Both the specimen carriage and impactor carriage run on guide rails. An air gun propels the impactor carriage down the guide rails towards the stationary specimen carriage. The ceramic bars collide well before the collision of the urethane holders. This produces compressive stress waves emanating from the impact faces which propagate in either direction. The compressive wave reflects in tension from the free boundary ends. After a finite time, a net tension stress will suddenly appear at the sharp precrack and the ceramic bars will slide through the urethane holders after the impact.

Since the stress level in the specimen is proportional to the impact velocity, an accurate laser velocity measurement system was used to measure the impact velocity. The stress level was inferred from the impact velocity using $\sigma_o = EV_o/2C_b$ which is derived based on an ideal bar wave theory. The stress level depends on the impact velocity, $V_o$, the elastic bar wave speed, $C_b$, and the modulus of elasticity, E. Details of the experimental setup as well as the data reduction procedure are given in References [6,7].

## 3. Experimental a(t) and $K_I^{dyn}(t)$ histories

This section presents the experimental results obtained from the impact system developed for this project. The first results are the crack length history plots and the $K_I^{dyn}$ graphs for two different ceramics which were the subject of this study.

The procedure presented in Reference [6,7] was used to obtain the crack length histories of the ceramic specimens impacted at velocities of approximately 5.8 and 10 m/s for each of the materials. The crack length histories are presented in Figures 3 and 4. The crack velocities increased with increasing impact velocity. The alumina and the composite material showed nearly the same crack velocities. The crack length varied almost linearly with time.

The dynamic stress intensity factor, $K_I^{dyn}$, for the two materials are shown in Figure 5 and 6. The fracture toughness increased with increasing impact velocities within each material group. The $K_I^{dyn}$ data was plotted as a function of the non-dimensional crack length, $\alpha = a/W$. Initially, $K_I^{dyn}$ increased rapidly and then increased more slowly at a constant rate.

## 4 Experiment Summary

The dynamic initiation fracture toughness, $K_{Id}$, was calculated by the technique presented in Reference [7]. The results are summarized in Table 2. The specimens impacted at 10 m/s showed macroscopic crack branching at the crack lengths, $a_b$, marked in Figures 5 and 6. The crack branch toughness[8], $K_{Ib}$, is also listed in Table 2 which is defined by $K_{Ib} = K_I^{dyn}$ at $a = a_b$.

Table 2 , Experiment Summary

| Material | $V_o$ m/s | V m/s | $V/C_2$ | $K_{IC}$ MPa$\sqrt{m}$ | $K_{Id}$ MPa$\sqrt{m}$ | $K_{Ib}$ MPa$\sqrt{m}$ |
|---|---|---|---|---|---|---|
| Hot Pressed | 5.7 | 1546 | 0.24 | 4 | 5.9 | - |
| $Al_2O_3$ | 10.1 | 2465 | 0.39 | | 5.8 | 13.6 |
| 29% vol. | 5.8 | 1536 | 0.23 | 7 | 6.5 | - |
| $SiC_w/Al_2O_3$ | 10.1 | 2383 | 0.36 | | 9.8 | 14.2 |

The initiation dynamic fracture toughness, $K_{Id}$, was in the range of previously published values for similar materials [9-12]. The technique for determining $K_{Id}$ requires the stress history at the crack tip to be correctly measured and the time at the initiation of crack propagation to be correctly determined from the LIDG signals. Surpassing $K_{Ib}$ was a necessary, but not sufficient condition for the crack to branch [8]. This was verified in this study since in other tests, $K_I^{dyn}$ exceeded $K_{Ib}$ without crack branching.

## 5. Fracture Surface Morphology

An emphasis of this paper is to use the scanning electron microscope to correlate the fracture surface morphology of the $Al_2O_3$ and the 29% v. $SiC_w/Al_2O_3$ composite with the experimental dynamic stress intensity factor curves. The value of $K_I^{dyn}$ increased four fold over $K_{Id}$ in both materials at the highest impact velocity. One would expect the fracture surface morphology to exhibit increased material damage with increasing $K_I^{dyn}$. Since the toughening mechanism in the composite was apparently ineffective, the lack of effective toughening must also be investigated. The difference between the quasi-static and dynamic fracture surface morphologies would also be of interest.

The fracture surfaces exhibited as many as five different distinct regions (See Figure 7). The first zone was the precrack region which showed a relatively flat and uniformly diffuse surface. Immediately following the precrack region was a narrow band of smooth surface which was named the "crack initiation" zone. The third region was a rough, relatively flat dynamic fracture region. The next surface

consisted of small localized crack branches (branching attempts) on a surface which was rough and of non-uniform shading. All materials impacted at 10 m/s exhibited a macro-branched region (5th region). The specimens impacted at 5.8 m/s did not display the macroscopic crack branch region. The initial crack was longer in the center section where plane strain conditions were dominant. Figure 8 is a mosaic of $Al_2O_3$ showing this fracture morphology. These regions were difficult to observe with the SEM or the optical microscope, but were more apparent with the naked eye.

A small zone of stable crack growth was sometimes present at the end of the precrack region. Microscopic surface features were compared with the surface in the dynamic fracture region. Figures 9 and 10 show an increased percentage of transgranular fracture in the dynamic fracture region. Both the quasi-static and the dynamic fracture surfaces of the $Al_2O_3$ exhibited a combination of intergranular and transgranular fracture surfaces where the intergranular fracture was dominant. Nevertheless, the dynamic fracture surface displayed a larger percentage of transgranular fracture surface. The high magnification photographs of the 29% v. $SiC_w/Al_2O_3$ revealed similar situations as shown Figures 11 and 12. The fracture surface exhibited both fiber pullout and trans-fiber fracture. The dynamic fracture regions had an increased percentage of trans-fiber fracture area. The apparent lack of increased fiber pullout and hence the lack in increased crack bridging toughening mechanism would help explain the nearly equal dynamic fracture toughness in the $Al_2O_3$ and the CMC.

Apparently, a more pronounced mechanism to increase the fracture toughness is to increase the fracture surface area. As the crack moves forward, the relatively flat surface becomes wavy. Next, the high stress intensity factor caused multiple fracture planes to be activated in front of the crack tip. The microscopic fracture surfaces join as the crack advances, forming many "branching attempts". An example of this type of branching attempt is shown in Figure 13. The crack advanced from bottom to top in the photograph which is evidence indicating a second crack plane forming ahead of the crack tip and then joining with the propagating macro-crack. A macroscopic crack branch successfully occurred in the specimens impacted at 10 m/s.

## 6. Discussion

The impact experiment is a valuable procedure for studying dynamic fracture of ceramic materials. The stress wave is essentially "trapped" in the bar specimen. As the crack propagates $K_I^{dyn}$ increases thus generating a variation in the fracture surface morphology. On the microscopic scale, increased areas of transgranular fracture in both $Al_2O_3$ and $SiC_w/Al_2O_3$ were observed. The macroscopic fracture features are more pronounced under the increasing stress intensity factor. After dynamic fracture initiation the fracture surface changes from a smooth surface to a rough surface, essentially increasing the fracture area. Next, multiple planes of fracture occur and join giving the appearance of crack branching attempts. Finally, a macroscopic crack branch occurs. The basic mechanism to accommodate the increased $K_I^{dyn}$ is to increase the fracture surface area as all the macroscopic features are caused by this mechanism. The microscopic transgranular fracture can dissipate only a limited amount of energy.

## 7. Conclusions

1. The fracture surface morphology of both the $Al_2O_3$ and the $SiC_w/Al_2O_3$ composite showed an increased percentage of transgranular fracture in the dynamic fracture zone.

2. The fracture surface displayed as many as five distinct fracture regions.

3. The ceramic materials accommodated the increasing stress intensity factor by increasing the the fracture area.

4. Multiple fracture surfaces formed ahead of the crack tip when the stress intensity factor was sufficiently high.

5. The toughening mechanism due to SiC whiskers in the $SiC_w/Al_2O_3$ composite were apparently ineffective under severe dynamic loading.

## 8. Acknowledgement

The authors gratefully acknowledge the financial support of the Office of Naval Research through ONR Contract N00014-87-K-0326. The scientific guidance and encouragement from Dr. Y. Rajapakse, ONR Scientific Officer, are greatly appreciated.

## 9. References

1. R.W. Rice, "Mechanisms of Toughening in Ceramic Matrix Composites," *Ceramic Engineering and Science Proceedings*, Vol. 2, No. 7-8, pp. 661-681, 1981.

2. W. N. Sharpe, Jr., Z. Waclawiw, and A. S. Douglas, "Dynamic Measurement of Crack-Tip Opening Displacement," *Fracture Mechanics: Nineteenth Symposium ASTM STP 969*, T. A. Cruse, Ed., American Society for Testing and Materials, Philadelphia, pp. 466-481, 1988.

3. M.G. Jenkins, A.S. Kobayashi, M. Sakai, K.W. White and R.C. Bradt, "Fracture Toughness Testing of Ceramics Using a Laser Interferometric Strain Gage," Bulletin of American Ceramic Society, Vol. 66, No. 12, pp. 1734-1738, 1987.

4. T. Nose and T. Fujii, "Evaluation of Fracture Toughness for Ceramic Materials by a Single-Edge-Precracked-Beam Method." *Journal of the American Ceramic Society*, Vol. 71 No. 5, pp. 328-333, 1988.

5. T. Sadahiro and S. Takatwu, "A New Precracking Method for Fracture Toughness Testing of Cemented Carbides," *Modern Developments in Powder Metallurgy*, Vol. 14, Eds. H.H. Hauser, H.W. Antes, and G.D. Smith, Metal Powder Industries Federation, Princeton, NJ, pp. 561-572, 1981.

6. L.R. Deobald, *Experimental/Numerical Characterization of the Dynamic Fracture Behavior of Ceramic Materials*, Ph.D. Dissertation, University of Washington, Seattle, WA, submitted June 1991.

7. L.R. Deobald and A.S. Kobayashi, "A Bar Impact Tester for Dynamic Fracture Testing of Ceramics and Ceramic Composites," Submitted to *Experimental Mechanics*.

8. M. Ramulu and A.S. Kobayashi, "Mechanics of Crack Curving and Branching," *International Journal of Fracture*, Vol. 27, pp. 187-201, 1985.

9. K.H. Yang and A.S. Kobayashi, "Dynamic Fracture Responses of Alumina and Two Ceramic Composites." *Journal of the American Ceramic Society*, Vol. 73, No. 8, pp. 2309-2315, 1990.

10. S. Suresh, T. Nakamura, Y. Yeshurun, K.-H. Yang, and J. Duffy, "Tensile Fracture Toughness of Ceramic Materials: Effects of Dynamic Loading and Elevated Temperatures," *Journal of the American Ceramic Society*, Vol. 73, No. 8, pp. 2457-2466, 1990.

11. Y. Takagi and A. S. Kobayashi, "Further Studies on Dynamic Fracture Response of Alumina and $SiC_w/Al_2O_3$ Composite," *Symposium on Elevated Temperature Crack Growth*, eds. S. Mall and T. Nicholas, ASME MD-Vol. 18, pp. 145-148, 1990.

12. J. Duffy, S. Suresh, K. Cho, E.R. Bopp, "A Method for Dynamic Fracture Initiation Testing of Ceramics," *Journal of Engineering Materials and Technology*, Vol. 110, pp 325-331, 1988.

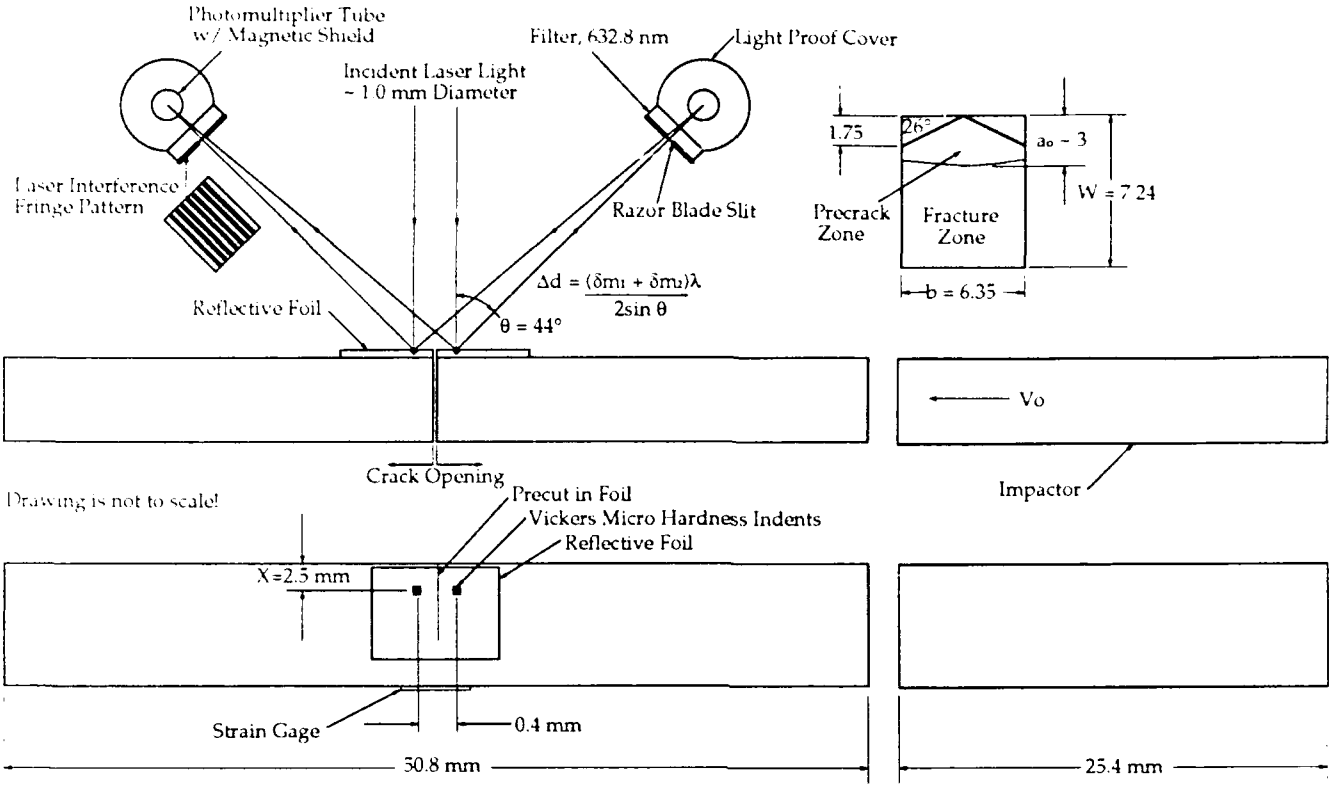


Figure 1, Specimen geometry and the LIDG technique.

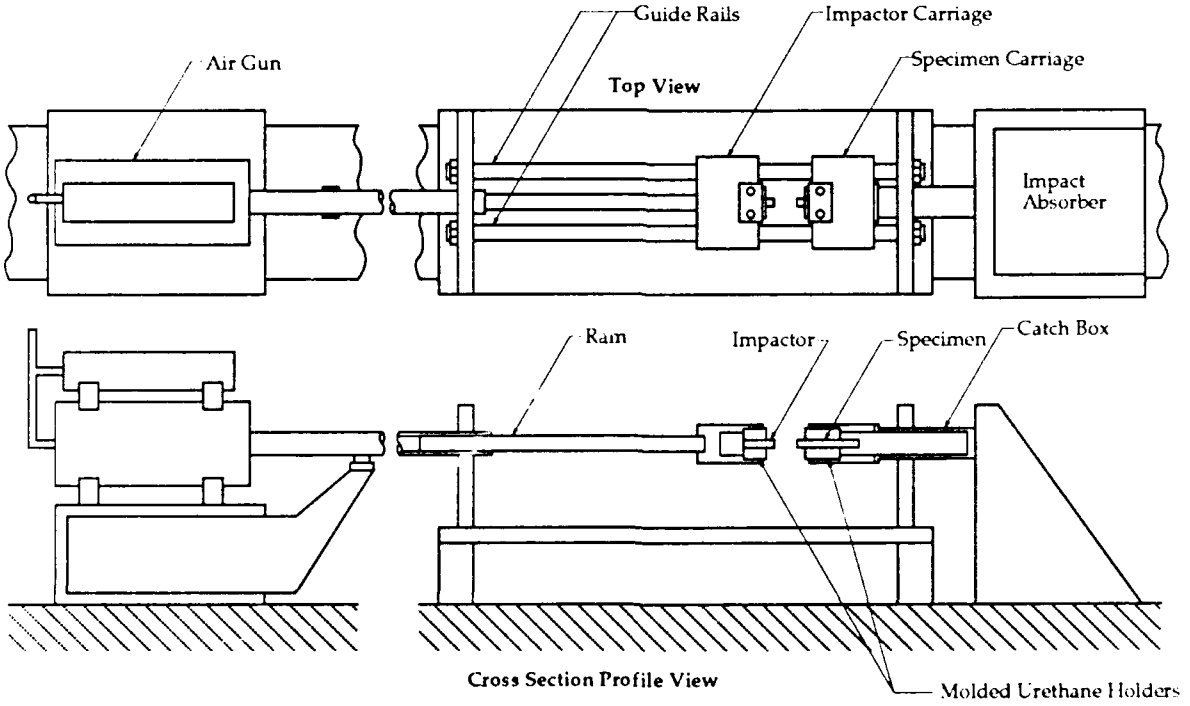


Figure 2, Impact apparatus and air gun.

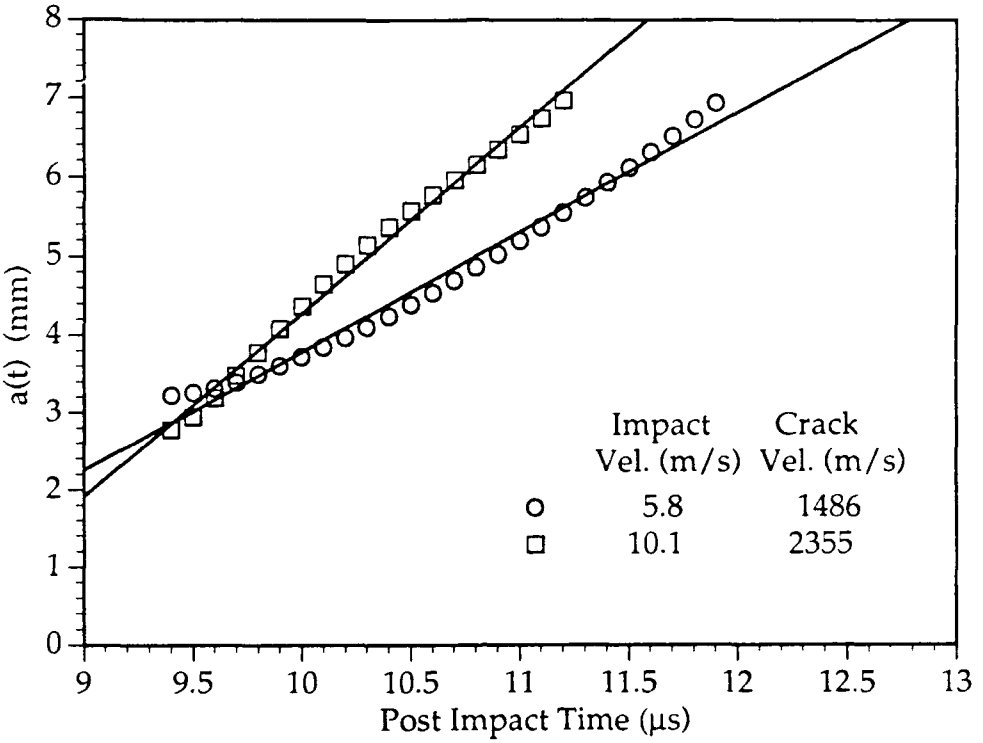


Figure 3, Crack length history for $Al_2O_3$.

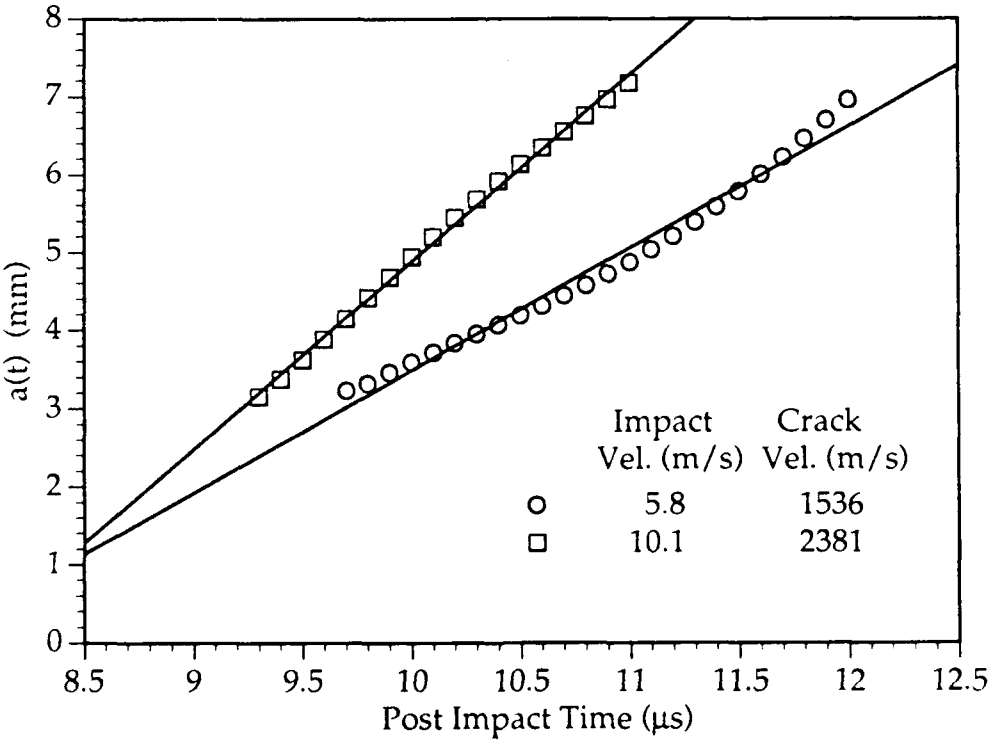


Figure 4, Crack length history for $SiC_w/Al_2O_3$ composite.

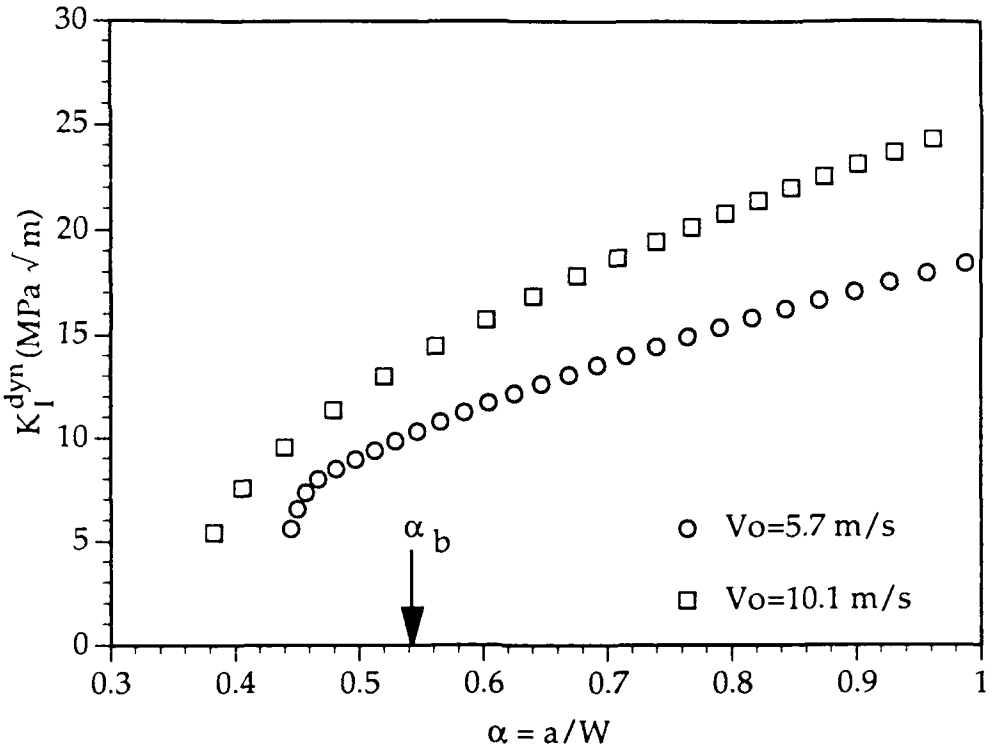


Figure 5, $K_I^{dyn}$ versus crack position, α=a/W for $Al_2O_3$.

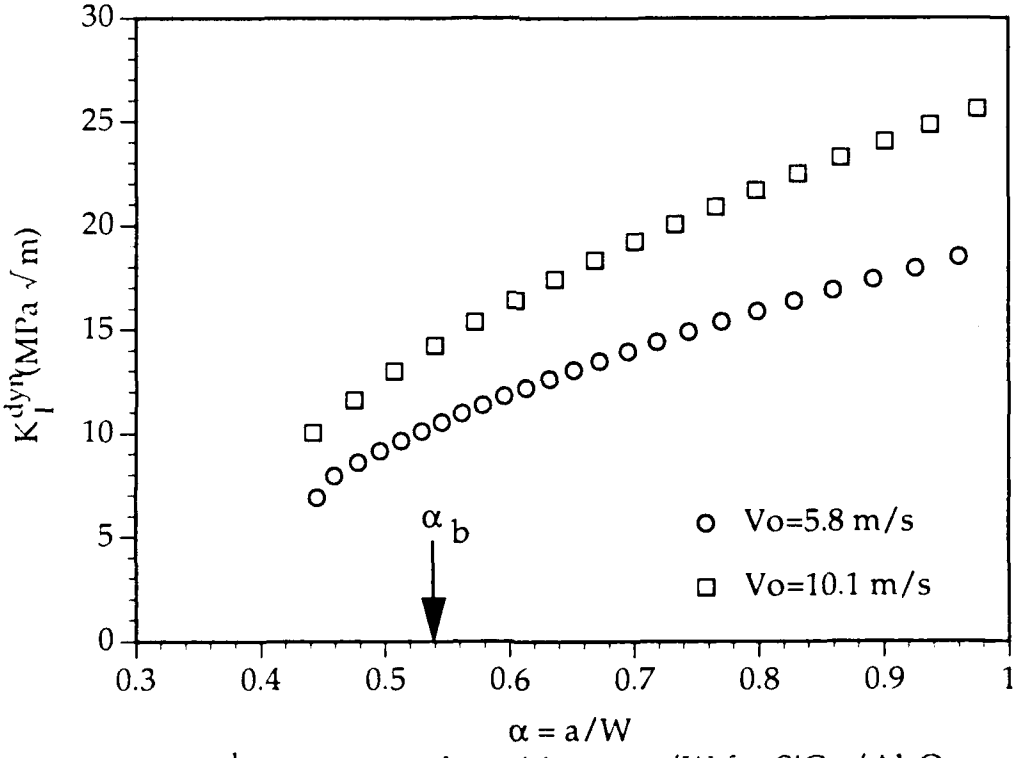


Figure 6, $K_I^{dyn}$ versus crack position, α=a/W for $SiC_w/Al_2O_3$ composite.

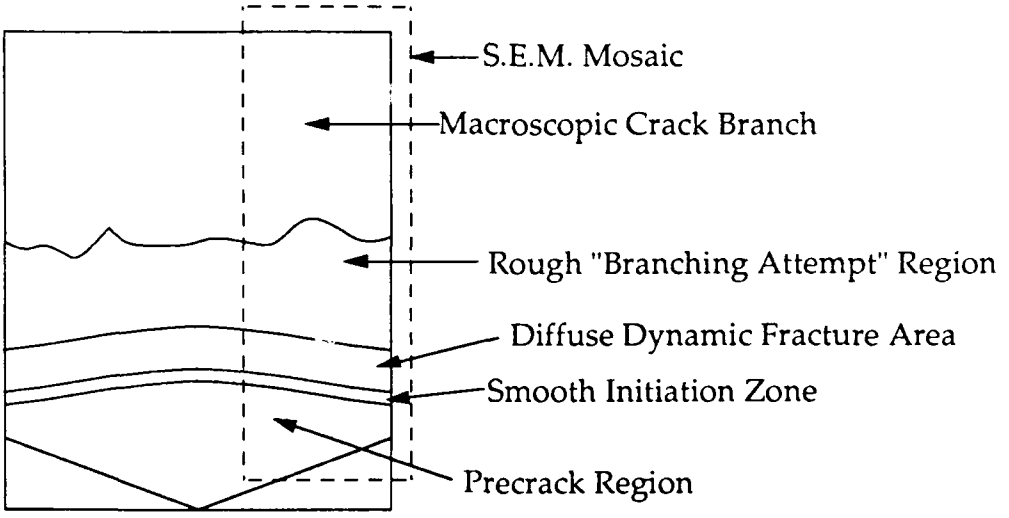


Figure 7, Schematic of fracture process regions on the ceramic bars.

Figure 8, S.E.M. mosaic of fracture morphology regions on $Al_2O_3$; magnification=35X.

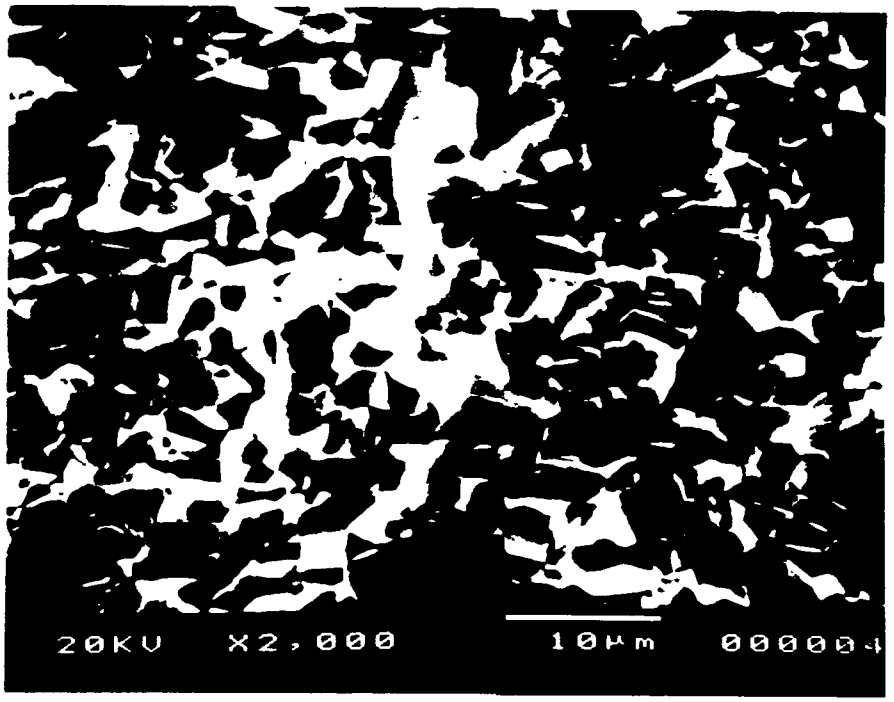


Figure 9, Intergranular quasi-static fracture in the $Al_2O_3$.

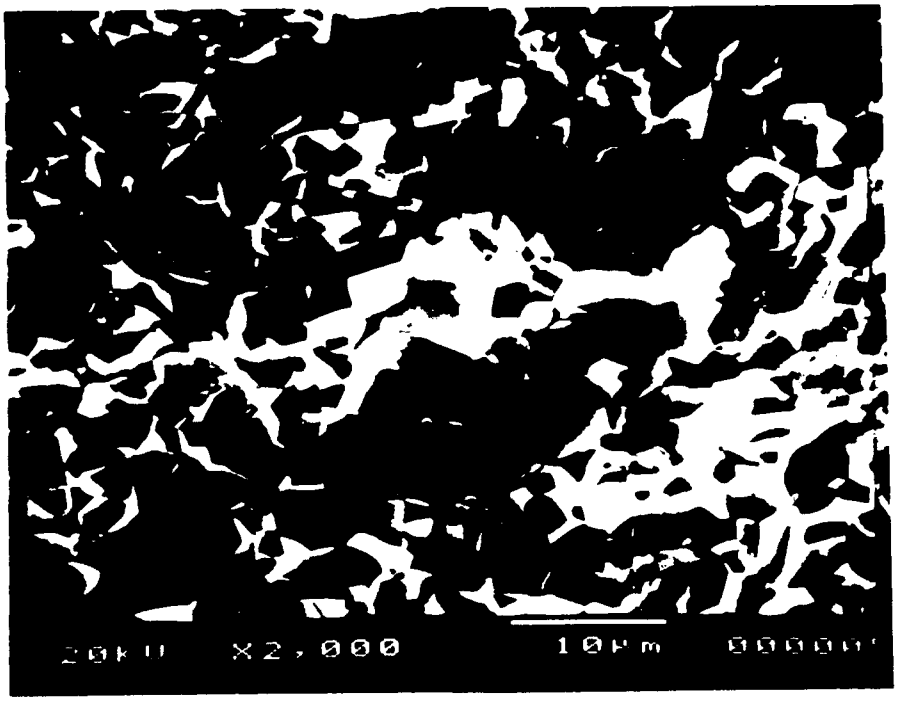


Figure 10, Transgranular dynamic fracture in the $Al_2O_3$.

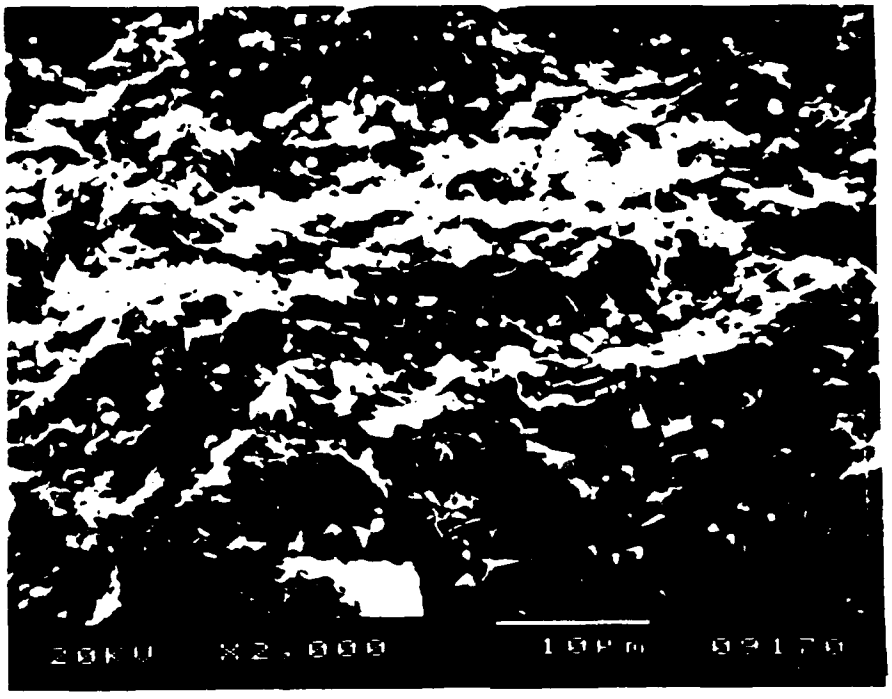


Figure 11, Fiber pullouts on the quasi-static fracture surface of $SiC_w/Al_2O_3$.

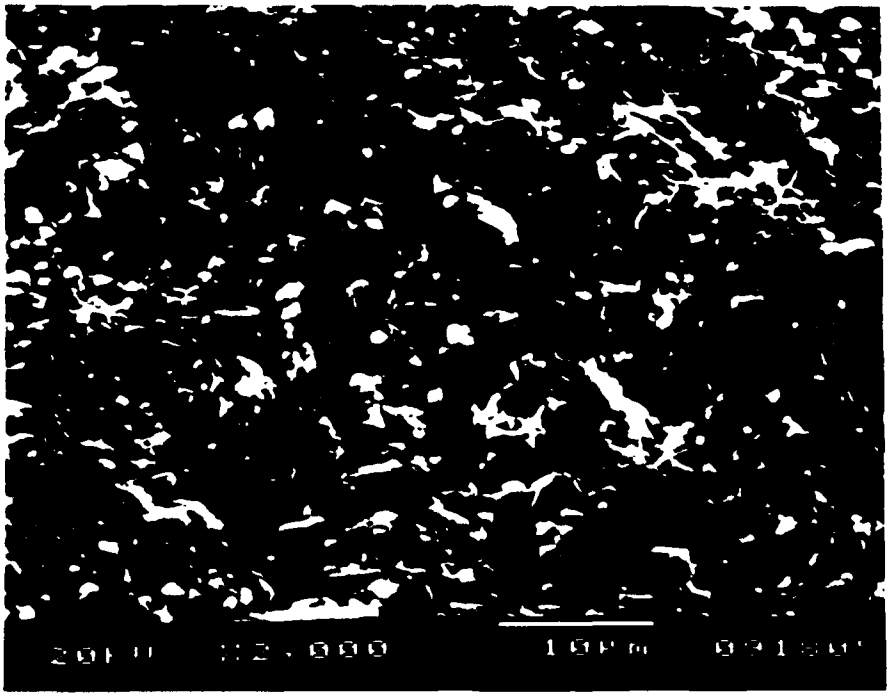


Figure 12, Trans-fiber dynamic fracture surface of $SiC_w/Al_2O_3$ composite.

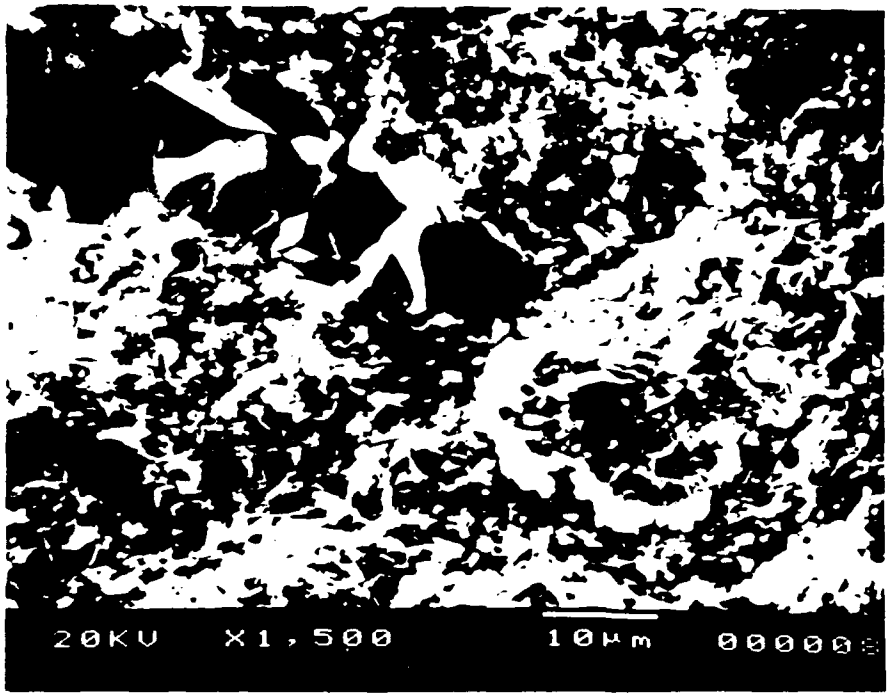


Figure 13, Branching attempt in the $SiC_w/Al_2O_3$ composite.

# REPORT DOCUMENTATION PAGE

Form Approved
OMB No. 0704-0188



| 1. AGENCY USE ONLY (Leave blank) | 2. REPORT DATE | 3. REPORT TYPE AND DATES COVERED |
|---|---|---|
| | October 1991 | Technical Report |

**4. TITLE AND SUBTITLE**
Dynamic Fracture Characterization of $Al_2O_3$ and $SiC_w/Al_2O_3$

**5. FUNDING NUMBERS**
s400050srh05

**6. AUTHOR(S)**
L.R. Deobald and A.S. Kobayashi

**7. PERFORMING ORGANIZATION NAME(S) AND ADDRESS(ES)**
Department of Mechanical Engineering, FU-10
University of Washington
Seattle, WA 98195

**8. PERFORMING ORGANIZATION REPORT NUMBER**
UWA/DME/TR-91/7

**9. SPONSORING/MONITORING AGENCY NAME(S) AND ADDRESS(ES)**
Office of the Chief of Naval Research
Arlington, VA 22217-5000

**10. SPONSORING/MONITORING AGENCY REPORT NUMBER**
N00014-87-K-0326

**11. SUPPLEMENTARY NOTES**

**12a. DISTRIBUTION/AVAILABILITY STATEMENT**
Unlimited

**12b. DISTRIBUTION CODE**

**13. ABSTRACT** (Maximum 200 words)

Rectangular bars of $Al_2O_3$ and 29% volume fraction SiC whisker/$Al_2O_3$ composite with sharp precracks were tested in a newly developed bar impact experiment. The strain history was monitored using a strain gage and the crack opening displacement (COD) history was recorded with the laser interferometric displacement gage (LIDG) technique. A new data reduction procedure produced information on the crack length history and the dynamic stress intensity factor, $K_I^{dyn}$. The fracture surface morphology was studied with a scanning electron microscope (SEM) and compared with the impact velocity and the $K_I^{dyn}$ history.

The crack history and $K_I^{dyn}$ curves for the $Al_2O_3$ and 29% v. $SiC_w/Al_2O_3$ composite were virtually the same indicating that the short SiC whiskers were ineffective under dynamic fracture. SEM study revealed five distinct fracture morphology regions with increased percentage area of transgranular fracture in the ceramic matrix of both the $Al_2O_3$ and the $SiC_w/Al_2O_3$ with rapid crack propagation. Also the high dynamic stress intensity factor caused multiple microscopic crack planes to form and then join as the crack advanced.

| 14. SUBJECT TERMS | 15. NUMBER OF PAGES 18 |
|---|---|
| | 16. PRICE CODE |

| 17. SECURITY CLASSIFICATION OF REPORT | 18. SECURITY CLASSIFICATION OF THIS PAGE | 19. SECURITY CLASSIFICATION OF ABSTRACT | 20. LIMITATION OF ABSTRACT |
|---|---|---|---|
| Unclassified | Unclassified | Unclassified | |